ACS OMEGA

Open Access

http://pubs.acs.org/journal/acsodf

Article

Investigating the Mechanism of Diethylenetriamine Pentamethylene Phosphonic Acid as a Depressant for Calcite Flotation of Fluorite

Haijun Wu, Chenhu Zhang,* Jing Zhang, Chengyong Wang, Peng Chen, and Shiwei Wang

Cite This: *ACS Omega* 2024, 9, 17354−17367

Read Online

ACCESS | Metrics & More | Article Recommendations

ABSTRACT: Fluorite and calcite have been attracting research attention for a long time. This paper reports on an investigation of the use of diethylene triamine pentamethylphosphonic acid (DTPMPA) as a chelating inhibitor. DTPMPA was used as a chelating inhibitor to study the flotation, separation, and adsorption behaviors of fluorite and calcite minerals. The microflotation experiment showed that the maximum separation of fluorite and calcite can be achieved with a DTPMPA dosage of 1.5 × 10^{-4} mol/L under weakly alkaline conditions (pH = 8). Zeta potential measurement, Fourier transform infrared spectroscopy, and X-ray photoelectron spectroscopy were used to confirm that DTPMPA was adsorbed on the surface of calcite, inhibiting NaOl adsorption. Additionally, density functional theory calculations showed that oxygen in the DTPMPA phosphate group formed the most stable bidentate binuclear adsorption configuration by chelating with calcium on the calcite surface. Through detection analysis and simulation calculations, the results showed that DTPMPA exhibited significantly weaker adsorption on fluorite compared to that on calcite, highlighting its selective inhibition ability on calcite.

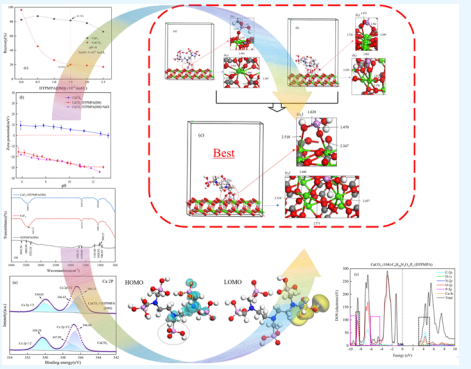

1. INTRODUCTION

Fluorite (CaF_2) has been considered to be a significant strategic mineral resource in recent years.[1] It has been applied in diverse ways in different industries, including chemical, metallurgy, glass/ceramics, and construction. However, natural deposits of fluorite often contain gangue minerals, such as barite ($BaSO_4$), calcite ($CaCO_3$), and quartz (SiO_2).[2] Among these, calcite is the primary gangue mineral associated with fluorite.[3] The similarities in their surface physical and chemical properties as well as their floatability make it difficult to separate fluorite from calcite effectively. Foam flotation, a physicochemical technique that employs mechanical agitation, has shown fluorite to be highly effective in selectively separating complex minerals based on their surface characteristics. Its remarkable performance in fluorite flotation is notable.[2,4]

In the foam flotation process, the addition of surfactants, such as collectors and inhibitors, is necessary. These surfactants serve to induce or inhibit the hydrophobicity of particles and facilitate the formation of stable foams.[2] Sodium oleate (NaOl) is a frequently used fatty acid as it possesses excellent harvesting capabilities and is readily available.[5,6] However, sodium oleate is not selective for fluorite and calcite. Given that fluorite and calcite have similar surface properties, introducing inhibitors in the fluorite−calcite system becomes necessary to achieve effective separation.[7] Flotation inhibitors are of two kinds: inorganic and organic. The commonly used inorganic inhibitors are water glass (Na_2SiO_3) and sodium hexametaphosphate $(NaPO_3)_6$. The disadvantages of inorganic inhibitors are the large amount of use and the reduction of the floatability of fluorite.[7,8] The use of large quantities of inorganic inhibitors increases the pollution of tailings and tailwater, making subsequent waste disposal more difficult.

Organic inhibitors have many advantages: they have a wide range of sources and are environmentally friendly and cheap.[9] In practical applications, organic inhibitors can be classified into two categories: small-molecule and large-molecule. Small-molecule organic inhibitors include citric, salicylic, tartaric, and lactic acid. These inhibitors commonly exhibit limited selectivity and inhibition ability, necessitating their combination to achieve the desired inhibitory effect.[10,11] On the other hand, macromolecules such as starch, dextrin, sodium lignosulfonate, sodium carboxymethyl cellulose, and tannin[12,13] offer good selectivity but are characterized by poor stability.

Received: January 3, 2024
Revised: February 18, 2024
Accepted: March 27, 2024
Published: April 8, 2024

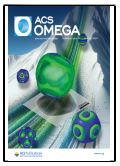

Recently, significant progress has been made in solving the problems of a large dosage and poor selectivity of these inhibitors. These improvements are achieved using chelating agents to form chelating compounds with specific metal ions through coordination chemical bonds. Chelates with five-membered or six-membered rings are considered to be stable, and the stability of the chelate increases with the number of atoms forming the ring.[14−17] Zhang et al. introduced pentasodium diethyltriamine pentaacetate (PD) as a new inhibitor, which effectively improved the recovery and separation of scheelite by flotation using fluorite and NaOl. The inhibitory effect was achieved through the chelation of PD with surface calcium in fluorite, enabling the separation of scheelite through flotation.[18] Chen and Tang used amino-trimethylenephosphonic acid (ATMP) as an inhibitor and NaOl as a collector for effective separation of calcite and magnesite.[19] These small-molecule chelating inhibitors, containing one or more phosphoric and carboxylic acid groups, exhibit high selectivity for calcite and possess strong chelating abilities. They address the issues associated with inorganic inhibitors like water glass, namely, the need for large quantities. In addition, they solve the problems associated with organic macromolecules and small molecules: those of instability and limited inhibition effectiveness. Further research is required to enhance our understanding of this class of chelating inhibitors.

Diethylenetriamine pentamethylene phosphonic acid (DTPMPA) is an organic compound belonging to the pentaphosphonic acid family. It is used as a water quality stabilizer and an organic phosphonic scale inhibitor. With its molecule containing multiple coordinate atoms, DTPMPA can form multicomponent ring chelates with various metal ions. These chelates disperse in water, disrupting the crystallization growth of the calcium salts. As a result, DTPMPA exhibits excellent scale-inhibition properties and finds wide applications in controlling the precipitation of carbonate,[20] phosphate, sulfate,[21] water, and iron oxide. DTPMPA is an environmentally friendly, cost-effective, and selectively advantageous scale inhibitor. Its exceptional calcium chelation ability makes DTPMPA a good candidate for use as an inhibitor with great potential for selectively separating fluorite and calcite. Therefore, our study of DTPMPA as an inhibitor for fluorite-calcite flotation separation is an important contribution to the field.

In this study, DTPMPA and NaOl were utilized as an inhibitor and a collector to perform flotation experiments on fluorite and calcite. The aim was to investigate the interaction of DTPMPA with these two minerals. The study of how the selective separation mechanism of the inhibitor affects both minerals was conducted with calculations of zeta potential measurements, Fourier transform infrared spectroscopy, X-ray photoelectron spectroscopy, and density functional theory.

2. MATERIALS AND METHODS

2.1. Minerals and Reagents. Fluorite and calcite were acquired from Hunan Shizhuyuan Nonferrous Metals Co., Ltd., China. Only pure minerals of −74 to +38 μm size were selected for the flotation experiments. The samples underwent repeated washing with ultrapure water and were dried at 100 °C before use. An X-ray diffraction (XRD) analysis was performed on the two samples. The XRD patterns, shown in Figure 1, display a high level of conformity with their respective standard reference specifications, showing that both minerals were very pure.

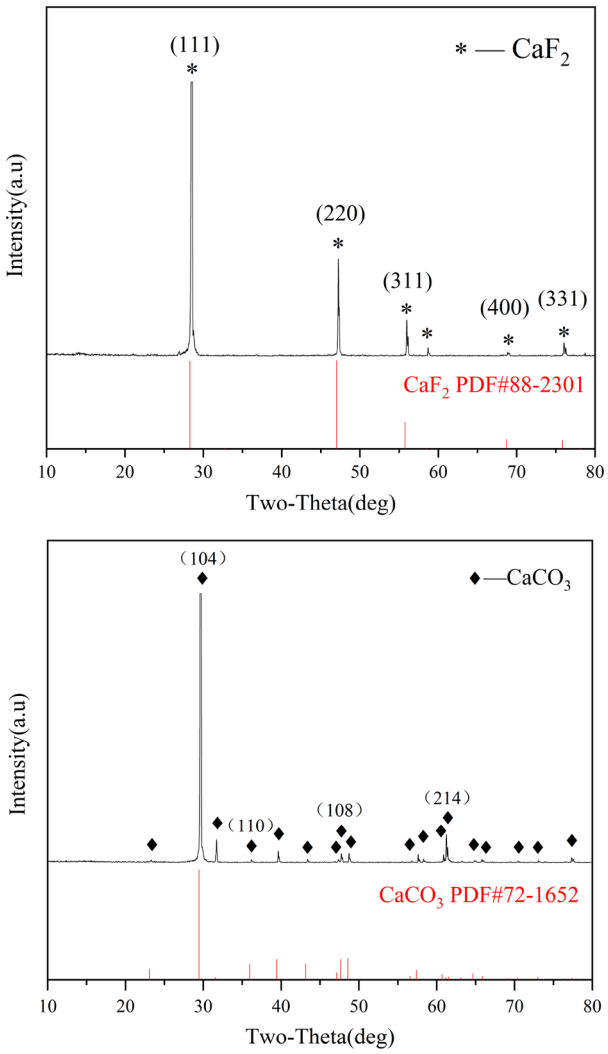

Figure 1. Fluorite and calcite XRD patterns.

The reagents used in this study were DTPMPA (DM), NaOl, HCl, and NaOH. All reagents were of analytical purity. In the flotation experiment, DM (shown in Figure 2) was used as an inhibitor, the organic molecular structure is shown in Figure 3, and NaOl served as the collector. The pulp pH was modified using HCl and NaOH, and ultrapure water with a resistance exceeding 18 MΩ × cm was utilized.

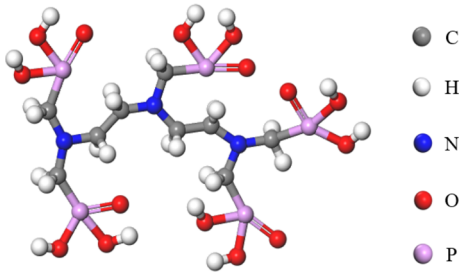

Figure 2. Three-dimensional structure of DTPMPA (DM).

2.2. Microflotation Experiment. The flotation experiment was performed using an XFG II hanging tank flotation machine (1500 r/min) manufactured by Wuhan Prospecting Machinery Factory. A 40 mL plexiglass tank was used for the

https://doi.org/10.1021/acsomega.3c10400
ACS Omega 2024, 9, 17354−17367

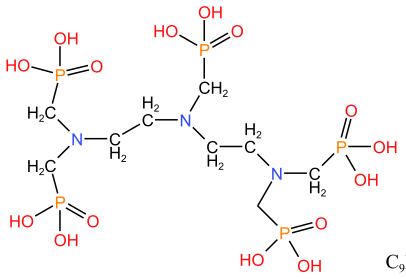

Figure 3. Molecular structure of the organic depressant DTPMPA (DM) for mineral flotation.

experiment. The experimental procedure was as described here: First, 2 g of pure ore samples was weighed and added to the flotation cell, along with 35 mL of ultrapure water. After the ore sample and water were thoroughly stirred, a pH meter was used to measure the pH of the initial pulp. Once the pH value stabilized, HCl or NaOH was added to adjust the pulp pH as desired for the experiment. The adjusted pH value was recorded for reference. Subsequently, an appropriate quantity of inhibitor DTPMPA (DM) was added and stirred for 2 min and the flotation collector NaOl was added for 2 min. After a 4 min interval, the foam floating on the liquid surface was carefully scooped. The collected foam was then filtered, dried, and weighed to determine its recovery rate. Each test was performed three times, with the mean value recorded as the representative value.

2.3. Zeta Potential Measurements. The ζ potential was measured at 25 °C with a Nano ZS90 analyzer (Malvern Zetasizer, UK). For the preparation of samples, 0.02 g of pure ore sample was put in a beaker, which contained 35 mL of a 1 × 10^{-2} mol/L KCl background electrolyte. The suspension's pH was regulated to a specific value using HCl or NaOH (concentrations of NaOl and NaOl + DTPMPA (DM)). After 5 min of stirring, the mineral suspension was allowed to settle for 5 min. The liquid phase was then separated and transferred to a test container to measure the ζ potential.

2.4. FTIR Measurements. The FTIR data detection was performed with a Bruker Alpha instrument (Thermo Fisher IS50, Thermo Fisher Scientific, Waltham, Massachusetts, USA) at an ambient temperature of 25 ± 1 °C. The sample was prepared as follows: At 25 °C, 0.2 g of pure fluorite/calcite ore sample was put in 35 mL of ultrapure water with a pH of 8. An inhibitor solution was also added with or without a 1.5 × 10^{-4} mol/L concentration. After 30 min of stirring and subsequent filtration of the supernatant from the minerals, the resulting mixture was placed in a vacuum oven to dry at 35 °C. Then, the dried sample was ground with KBr in a 1:100 ratio to prepare a tablet. Finally, the prepared semitransparent flake was subjected to infrared testing.

2.5. XPS Analysis. An America Thermo ESCALAB 250XI spectrometer was used to examine the fluorite and calcite XPS spectra pre- and post-treatment with DTPMPA (DM). The X-ray source used was monochrome Al Ka and rated 150 W. The collected spectra were of high resolution. A step size of 0.05 eV was used to collect the spectra. For sample preparation, a 0.2 g mineral sample was added to a 35 mL aqueous solution with or without DM (1.5 × 10^{-4} mol/L) at pH 8. The mixture was stirred at 25 °C for 0.5 h and then filtered. Deionized water was subsequently used to wash the mixture, which was then dried in vacuum at room temperature for 24 h. For the calibration of all elements, C 1s was utilized (284.80 eV).

2.6. DFT Calculations. All properties were calculated by using the CASTEP and DMol3 modules within Materials Studio 2020 software. The molecular structure optimization of DTPMPA (DM) and the crystal and surface optimization of fluorite and calcite minerals were performed in the CASTEP module. The adsorption model of DM on the mineral surfaces and the corresponding property calculations were conducted with the CASTEP module. The molecular properties of DM were calculated by using the DMol3 module. Considering the fluorite and calcite surface stabilities, two study surfaces were used: fluorite (111) surface[3,22,23] and calcite (104) surface.[3,24]

The calculation of fluorite and calcite unit cell models was performed using the Build Crystals module in Materials Studio 2020 (Figure 4). The parameters for the unit cell models were

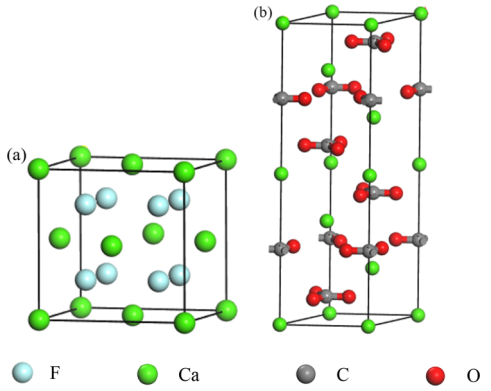

Figure 4. (a) Fluorite and (b) calcite cells.

obtained from the American Mineralogist Crystal Structure Database.[25] The parameters for the fluorite unit cell are as follows: $a = b = c = 0.54631$ nm, $\alpha = \beta = \gamma = 90°$, space group $Fm\bar{3}m$, and $Z = 4$, belonging to the cubic crystal system.[26] The parameters of the calcite unit cell are a, $b = 0.4990$ nm, $c = 1.70615$ nm, α, $\beta = 90°$, and $\gamma = 120°$. The space group is R-3C, and calcite belongs to the trigonal crystal system.[27] The calculations of the DFT were within the generalized gradient approximation and performed using the PBE functional.[28,29]

The adsorption energy of the agent interacting with the mineral surface was obtained as follows:

$$E_{ads} = E_{complex} - E_{surf} - E_{DTPMPA}$$

where E_{ads} represents adsorption of mineral surface adsorbent, $E_{complex}$ represents the total energy of complex formed through adsorption of mineral surface adsorbent, and E_{surf} and E_{DTPMPA} represent mineral surface total energy and adsorbent total energy,[30] respectively.

3. RESULTS AND DISCUSSION

3.1. Microflotation Results. In single-mineral flotation, the mineral flotation recovery depends on the slurry pH and reagent dosage.[31] DTPMPA (DM) was used as the inhibitor, and NaOl was used as the collector. Flotation tests were conducted for pH, DM, and NaOl dosage, and the results were as shown in Figures 5 and 6, respectively.

For fluorite and calcite without DM, Figure 5 illustrates the flotation mechanism. In Figure 5a, the flotation recovery change of fluorite and calcite with pH is illustrated at a concentration of 3 × 10^{-4} mol/L NaOl. The recovery rate of both minerals gradually increased with increasing pH. Specifically, the recovery rate of fluorite shows a significant

https://doi.org/10.1021/acsomega.3c10400
ACS Omega 2024, 9, 17354−17367

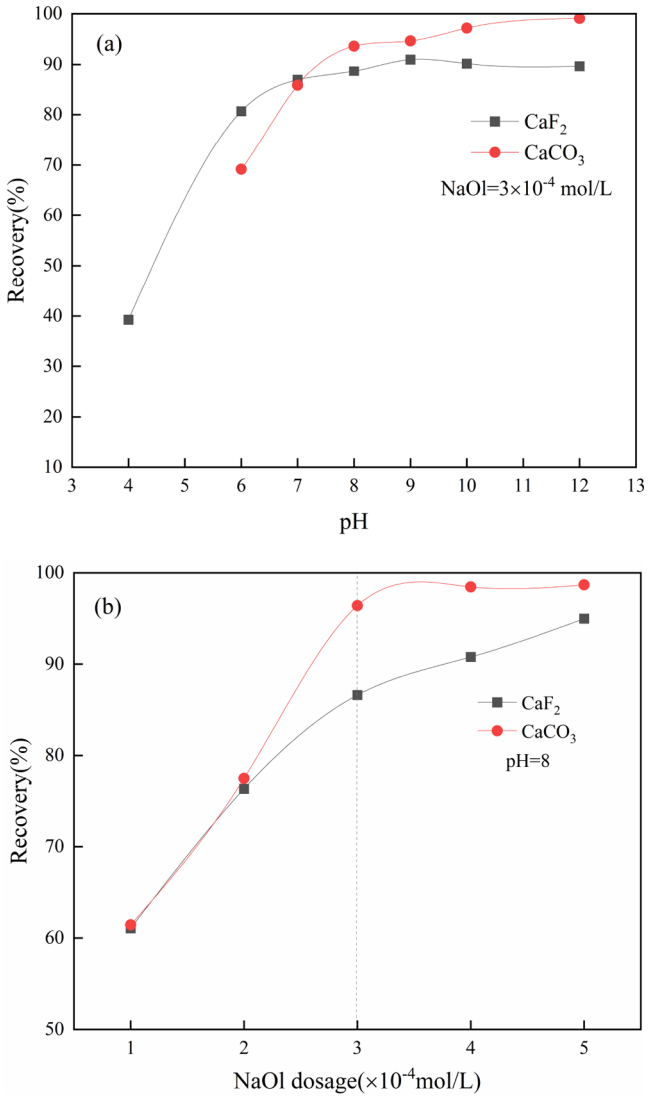

Figure 5. (a) Effect of pH and (b) NaOl dosage on the flotation recovery of fluorite and calcite.

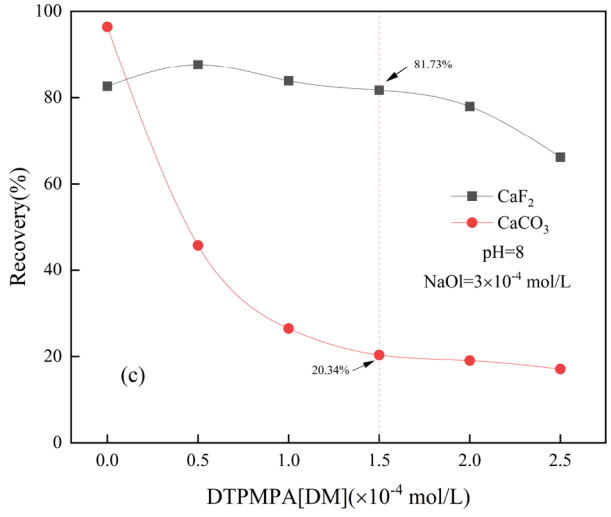

Figure 6. Influence of DTPMPA (DM) dosage on the flotation behavior of fluorite and calcite (NaOl: 3×10^{-4} mol/L; pH: 8).

increase between pH 4 and 8, reaching a stabilization point when the pH exceeds 8. On the other hand, the recovery rate of calcite exhibits a rapid rise between pH 6 and 8 and it rises slightly in the pH range of 8−12. Clearly, the optimal flotation conditions for both minerals were pH 8.

As Figure 5b illustrates, the floatability of fluorite and calcite was considerably enhanced at a NaOl concentration range of 1.0×10^{-4} to 3.0×10^{-4} mol/L, with an optimal pH of 8. Specifically, when NaOl reached a concentration of 3×10^{-4} mol/L, both minerals exhibited the greatest flotation recovery disparity with subsequent changes being minimal. Notably, higher concentrations of NaOl did not yield a significant increase in floatability. Therefore, the ideal flotation condition requires a NaOl concentration of 3.0×10^{-4} mol/L and pH of 8. These flotation results indicate the difficulty of separating the two minerals without the addition of inhibitors under the optimum pH of 8.

Figure 6 illustrates how the DM dosage affects the recovery rates of flotation for both minerals. The floatability of fluorite and calcite was examined using varying concentrations of DM while maintaining a fixed NaOl collector concentration and pH. Increasing the DM dosage dropped the calcite recovery rate. However, the decrease in recovery rate was more prominent for calcite than for fluorite. At a DM concentration of 1.5×10^{-4} mol/L, the recovery rate of calcite was only 20.34% whereas the recovery rate of fluorite reached 81.73%. This observation suggests that DM effectively separates fluorite from calcite under these experimental conditions.

3.2. Zeta Potential Results. In flotation, the surface structure properties of minerals have a vital influence on the adsorption of various flotation agents, thereby influencing the effectiveness of mineral separation using flotation techniques. The characterization of mineral surface properties is usually performed through a zeta potential measurement, which reflects the electrical charge distribution at the mineral surface. This potential value varies with the adsorption of different agents, enabling us to infer the adsorption strength of these agents on mineral surfaces.[32] Figure 7a,b illustrates the change in zeta potential with different pH values when two agents (DTPMPA (DM) and NaOl) were added to the fluorite and calcite mixture and when only one agent (either DM or NaOl) was added. As indicated by both data graphs, the potential differences are obvious in the flotation trends of the two minerals.

Figure 7a illustrates that the isoelectric point measurement of raw fluorite, which was determined to be 8.3, is consistent with previous research findings.[33] As Figure 7a shows, the surface of raw fluorite exhibited a positive charge within a pH range of 2−8 and a negative charge within a pH range of 8−13. Adding NaOl lowered the surface potential of fluorite by approximately −39.72 mV. The result indicates that NaOl at pH = 8 had stronger adsorption activity on fluorite. When both DM and NaOl were added, the negative potential decreased by approximately 6 mV compared to that when only NaOl was added, indicating that NaOl adsorption was slightly impacted by the inhibitor introduced. The inhibitor had some adsorption activity but was only slightly less than the value when only NaOl was added, which suggests that the adsorption activity of DM on fluorite was small. This phenomenon may be caused by the adsorption of NaOl on fluorite, which inhibits subsequent DM adsorption.

The effect of an inhibitor DM on the surface potential change of calcite with NaOl was investigated. The investigation

https://doi.org/10.1021/acsomega.3c10400
ACS Omega 2024, 9, 17354−17367

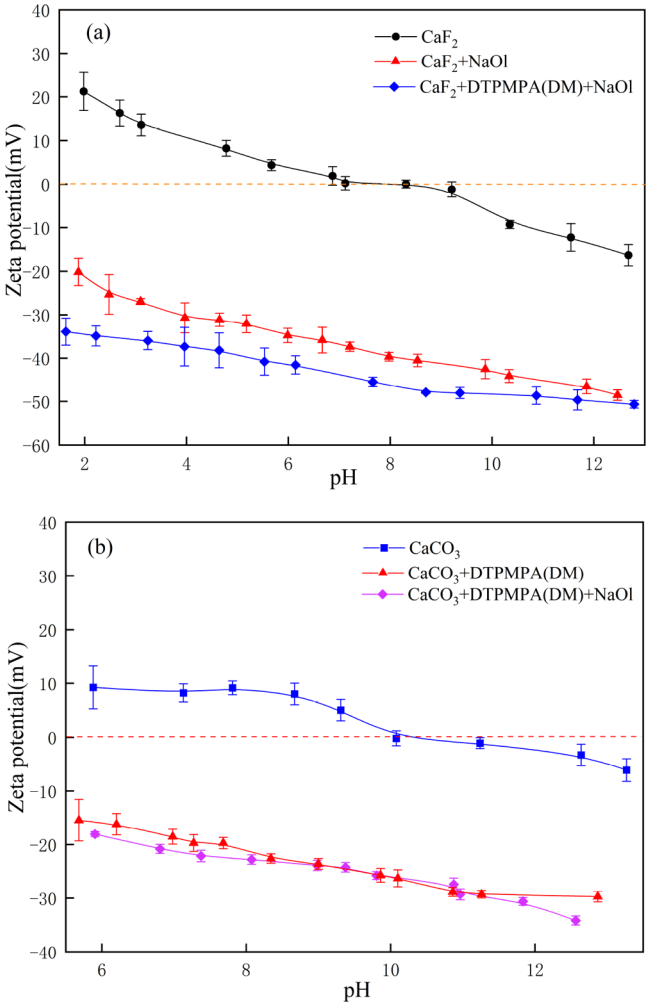

Figure 7. Effects of adding different reagents on the zeta potentials of (a) fluorite and (b) calcite (NaOl = 3 × 10^{-4} mol/L; DTPMPA (DM) = 1.5 × 10^{-4} mol/L).

was based on whether the inhibitor DM was present. As shown in Figure 7b, the measured isoelectric point of pure calcite is 10.2. In the range of the isoelectric point of calcite, the surface of calcite is positively charged in the range of pH 6−10.2 and negatively charged in the range of pH 10.2−13. Figure 7b illustrates the results. When only DM was added, the zeta potential on the calcite surface reduced from 8.7 to −30.2 mV, indicating a reduction of 21.5 mV. In contrast, when NaOl and DM were simultaneously added, the zeta potential on the calcite surface showed a smaller reduction of 1.31 mV (from −21.52 to −22.83 mV), suggesting that both potentials remained relatively unchanged. Thus, NaOl adsorption on calcite was significantly hindered after treatments with the inhibitor DM and collector NaOl. One explanation is that inhibitor DM occupies the active site on the surface of calcite and prevents the adsorption of NaOl. It is also possible that DM forms a film on the calcite surface, consequently inhibiting the subsequent adsorption of NaOl. Notably, the NaOl adsorption on the calcite surface was considerably weaker than that of fluorite because of the inhibitor, further supporting the NaOl adsorption hindrance. To further confirm these findings, FTIR and XPS analyses were conducted.

3.3. FTIR Results. The zeta potential measurements indicate selective adsorption of DTPMPA (DM) on the calcite surface. Thus, FTIR was also used to investigate how DM interacts with fluorite and calcite surfaces.

Figure 8a shows the CaF_2 FTIR spectra pre- and postaddition of DM. Upon adding DM, the peaks were at

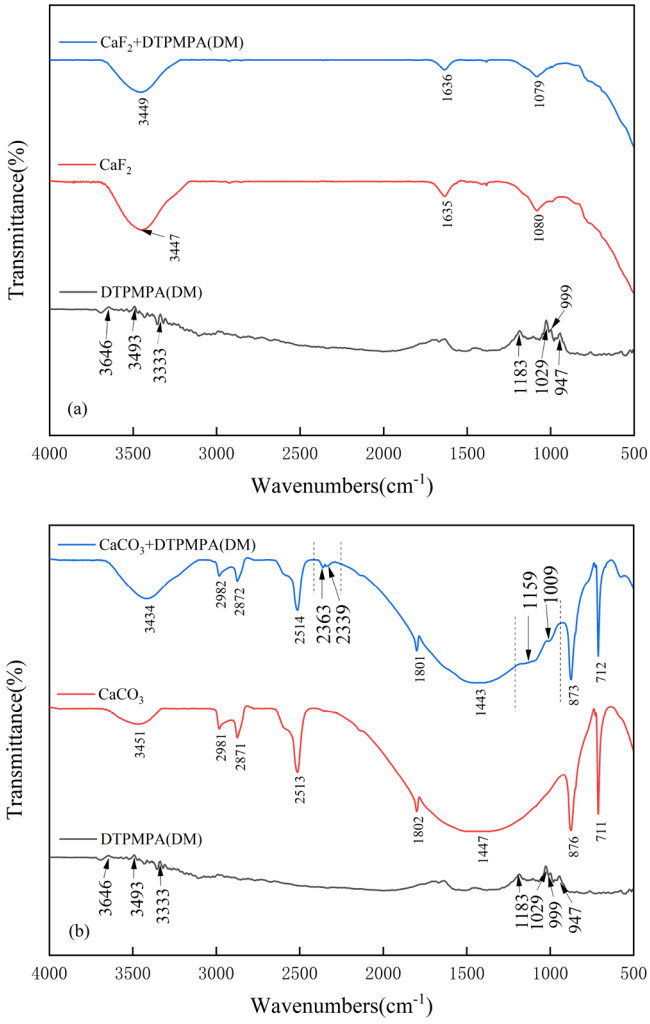

Figure 8. FTIR spectra of (a) fluorite and (b) calcite before and after the interaction with DTPMPA (DM).

3646, 3493, and 3333 cm^{-1}, corresponding to the tensile vibration of free —OH, intramolecular hydrogen bonding —OH, and intermolecular hydrogen bonding —OH, respectively. While the peaks at 1697 and 1641 cm^{-1} indicate −OH stretching and deformation vibrations on organic phosphate groups, the peak at 1183 cm^{-1} represents the stretching vibration of P−O.[31] Similarly, the peaks at 1029 and 999 cm^{-1} correspond to P−O stretching vibration while that at 947 cm^{-1} represents the expansion vibration of P−C. Figure 8a also shows the characteristic peaks of fluorite at 3447, 1635, and 1080 cm^{-1}, respectively.[7] The corresponding peaks at 3449, 1637, and 1079 cm^{-1} suggest that the peak frequencies on the surface of fluorite remained largely unchanged after treatment with DM, no new peaks were found, and only slight movement of the original peaks on the fluorite showed the action of the agent, indicating that DM did not interact with the fluorite surface.

Figure 8b depicts $CaCO_3$ FTIR spectra pre- and post-DM treatment. The figure shows the characteristic peaks of calcite

https://doi.org/10.1021/acsomega.3c10400
ACS Omega 2024, 9, 17354−17367

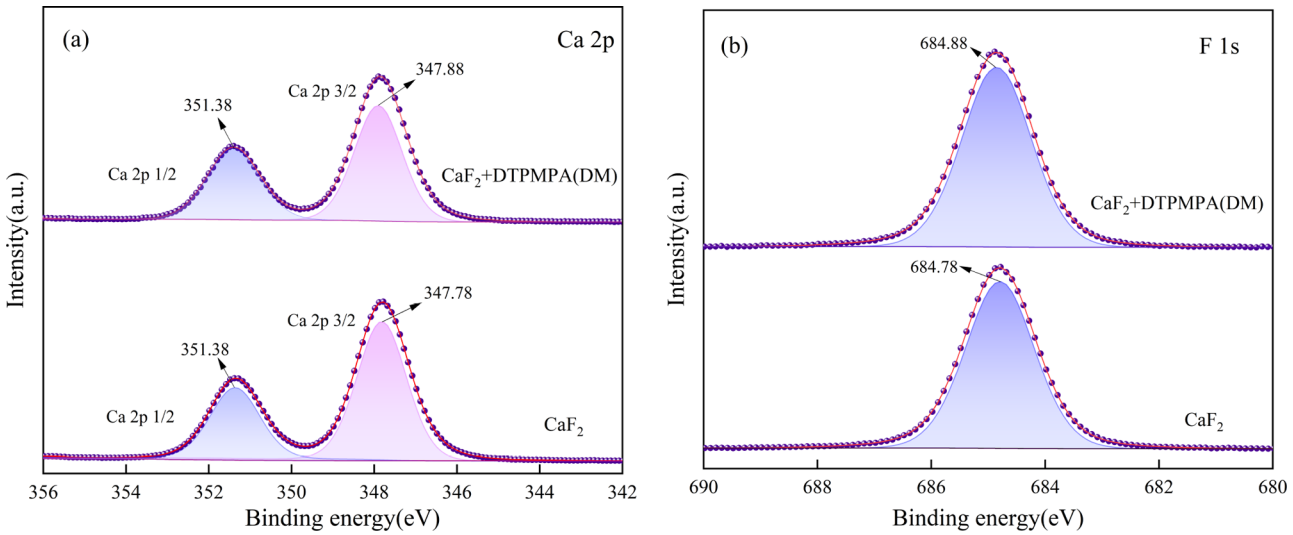

Figure 9. Fluorite high-resolution (a) Ca 2p and (b) F 1s XPS spectra recorded for fluorite pre-DTPMPA (DM) and post-DTPMPA (DM) processing.

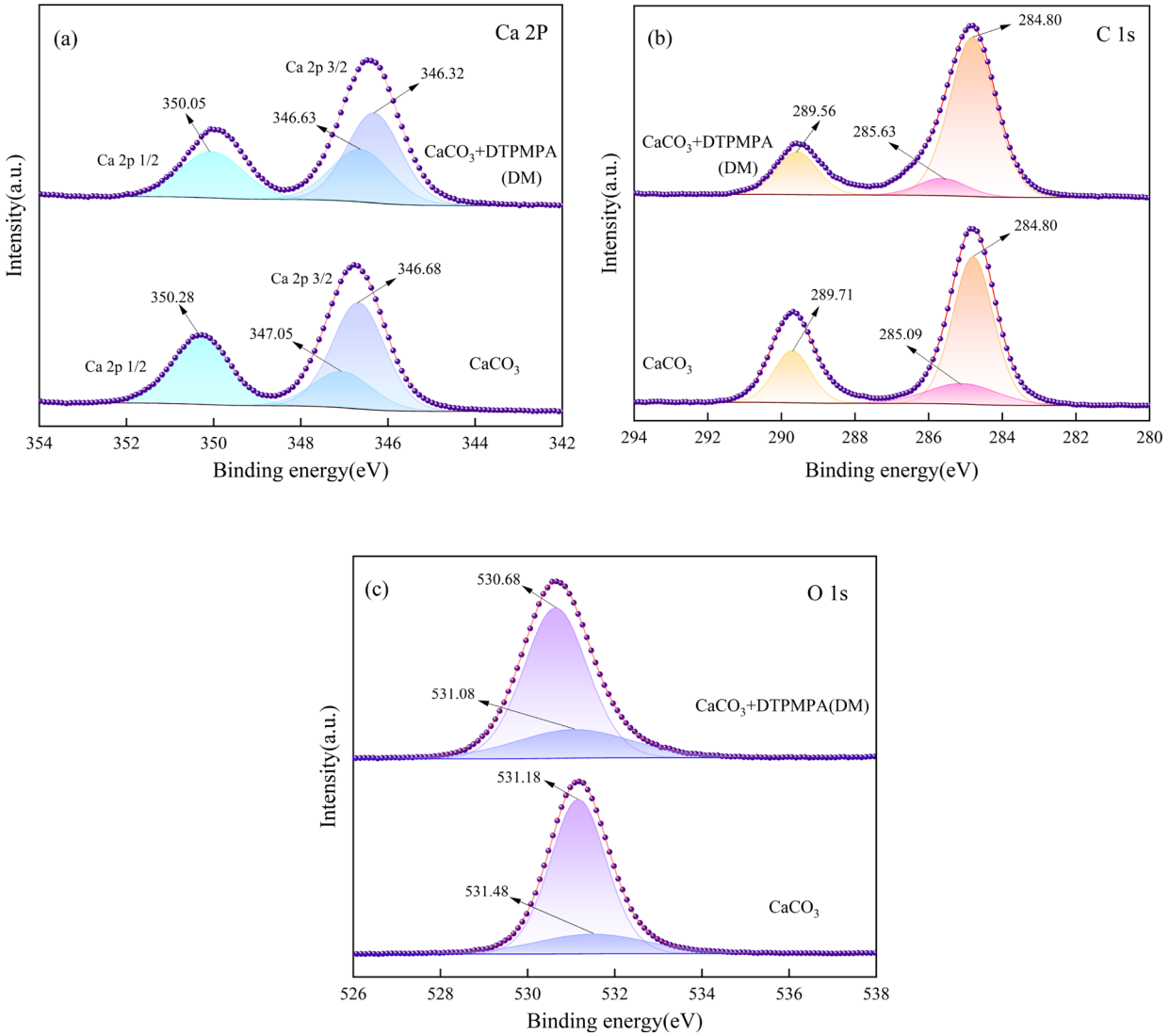

Figure 10. Calcite high-resolution (a) Ca 2p, (b) C 1s, and (c) O 1s XPS spectra recorded for fluorite pre- and post-DTPMPA (DM) processing.

https://doi.org/10.1021/acsomega.3c10400
ACS Omega 2024, 9, 17354−17367

at 3451, 2981, 2871, 2513, 1802, 1447, 876, and 711 cm^{-1}.[34,35] Notably, after treatment with DM, four new peaks emerged in the calcite spectrum: 2363, 2339, 1159, and 1009 cm^{-1}, respectively. The calcite surface, which appears as peaks at 2363 and 2339 cm^{-1}, corresponds to the tensile vibrations of O═C═O. These characteristic peaks did not appear when the inhibitor DM was used, which was mostly attributed to the error caused by atmospheric CO_2 pollution.[36] The peak at 1159 cm^{-1} indicates the P═O vibration on the organic phosphate group, while the peak at 1009 cm^{-1} represents the P−O vibration. Comparisons between DM-treated calcite and pure DM revealed changes in peak values. The peak at 1183 cm^{-1} reduced by 24 to 1159 cm^{-1}, and the peak at 1029 cm^{-1} reduced by 20 to 1009 cm^{-1}. Moreover, the peak at 3451 cm^{-1} of DM-treated calcite reduced by 17 to 3434 cm^{-1}, indicating the interaction between —OH on DM and Ca on the calcite surface. These results demonstrate the chemical adsorption of DM onto calcite, whereas no significant interaction between fluorite and DM was observed.

3.4. XPS Results. XPS is a widely used technique for determining the composition and chemical state of elements on mineral surfaces, making it a crucial method for surface analysis.[31] Figure 9 displays the Ca 2p narrow-scan spectrum of fluorite before and after DTPMPA (DM) treatment. The interaction of DM with both minerals was studied by selecting Ca 2p 3/2. The choice was based on the fixed energy difference between Ca 2p 3/2 and Ca 2p 1/2.[37]

Figure 9a shows that the Ca 2p 3/2 binding energy of fluorite increased from 347.78 to 347.88 eV after DM treatment, indicating a minimal increase of 0.1 eV. This increase can be attributed to instrument error (±0.1 eV) and can be disregarded.[31] The change in the chemical state of the Ca sites on fluorite was not significant. Therefore, the impact of DM on the chemical state of Ca atoms on fluorite is deemed to be weak and negligible. As Figure 9b illustrates, the broken chemical bond on fluorite is the Ca−F bond. The F 1s binding energy of fluorite shows a negligible increase of 0.1 eV (from 684.78 to 684.88 eV) after DM treatment. Therefore, it can be concluded that DM does not chemically adsorb on fluorite, which aligns with the findings of the FTIR analysis (Figure 7). Conversely, when comparing bare calcite (Figure 10a) to calcite treated with DM, a significant chemical reduction in the Ca 2p 3/2 peak binding energy is observed, measuring 0.36 and 0.42 eV (from 346.68 to 346.32 eV and from 347.05 to 346.63 eV), respectively. This suggests a stronger interaction between the Ca sites in DM and calcite compared with that in DM and fluorite.

The chemical bond broken by calcite is the Ca−O bond. Hence, aside from the role of Ca active sites in calcite minerals, researchers have also used the O active site of the active site to examine how DM adsorbs on calcite minerals. Figure 10c shows the XPS narrow-scan spectrum of calcite at the O 1s pre- and post-treatment of DM. Upon addition of DM, the two peak binding energies of the experimental O 1s of calcite in Figure 10c reduced by 0.5 and 0.4 eV, respectively (from 531.18 to 530.68 eV and 531.48 to 531.08 eV). This result indicates a stronger chemical interaction between DM and calcite than with DM and fluorite. Peak fitting analysis of the calcite C 1s spectrum also revealed a slight increase of 0.54 eV in the peak chemical state before and after the action of DM on calcite (from 285.09 to 285.63 eV), suggesting the presence of a C−O chemical structure in this energy range. The strong force exerted during DM's interaction with the Ca active site on the calcite surface changes the C−O binding energy of calcite.

The results demonstrate that robust calcite surface DM chemisorption impeded NaOl adsorption on calcite. DM exhibited significant chemical adsorption on calcite, consistent with the FTIR analysis. A microsimulation study was subsequently performed to determine how DM adsorbs on fluorite and calcite surfaces, further elucidating the adsorption mechanism on these mineral surfaces.

3.5. Computational Results. DFT is commonly used in the field of flotation for investigating surface adsorption at the molecular and atomic levels.[38] It enables researchers to explore the interactions between molecules, ions, and mineral surfaces, offering insights into the mechanisms underlying the adsorption of reagents onto minerals.[38−42] In the context of mineral flotation, DFT is frequently used for calculating and optimizing the structures and electronic properties of flotation reagent molecules. This usage enables a detailed examination of the binding affinity between reagents and metal ions on the mineral surface at a microscopic level. Leveraging DFT and quantum chemical calculation methods can yield a comprehensive understanding of the inhibitory mechanism of DTPMPA (DM) on mineral surfaces.

3.5.1. Frontier Molecular Orbital Analysis and Mulliken Population Analysis. DM was investigated to determine how it adorbs on mineral surfaces. According to Kenichi Fukui's frontier molecular orbital theory proposed in 1952,[43] the highest occupied molecular orbital (HOMO) of DM molecules corresponds to the central atom of the molecule. The activity of electrons is directly related to their energy, with higher HOMO values indicating stronger electron-providing abilities of the inhibitor molecules to the mineral surface, which then results in stronger interactions between the agents and the mineral surface. Moreover, molecular reactivity primarily relies on the HOMO and the lowest unoccupied molecular orbital (LUMO).[44]

The molecular structure diagrams of HOMO (Figure 11a) and LUMO (Figure 11b) of DM were obtained using the $Dmol_3$ module of Materials Studio 2020. According to the results, phosphate group oxygen atoms, specifically those in P═O and P−O bonds, are the primary electron-donating atoms in the HOMO of the DM inhibitor. Additionally, the O atoms in the —OH and P═O groups serve as the chemical reaction centers, actively participating in the inhibitor adsorption reaction on the mineral surface. They act by transferring electrons to the metal atoms on the surface. Notably, the 2p orbital of the O atom in DM, particularly in the HOMO, makes a considerable contribution to electron transfer for the formation of new covalent bonds with the mineral metal atoms.[45]

Since the HOMO orbital on DM is limited by steric hindrance during the optimization process, its adsorption occurs on the phosphoric acid group marked with a black circle in the HOMO diagram in Figure 11a, which is used as the active group adsorbed by the agent. During the inhibitor−mineral reaction, the HOMO of the inhibitor donates its electrons to the LUMO of the mineral, facilitating the formation of stable covalent bonds.[46] Furthermore, LUMO also receives a contribution from the oxygen atoms in the —OH group of the phosphoric acid and the P═O group. The —OH presence in the functional phosphoric acid group increases the contribution of the LUMO. The metal atoms on the mineral surface have abundant d-orbital electrons, which

https://doi.org/10.1021/acsomega.3c10400
ACS Omega 2024, 9, 17354−17367

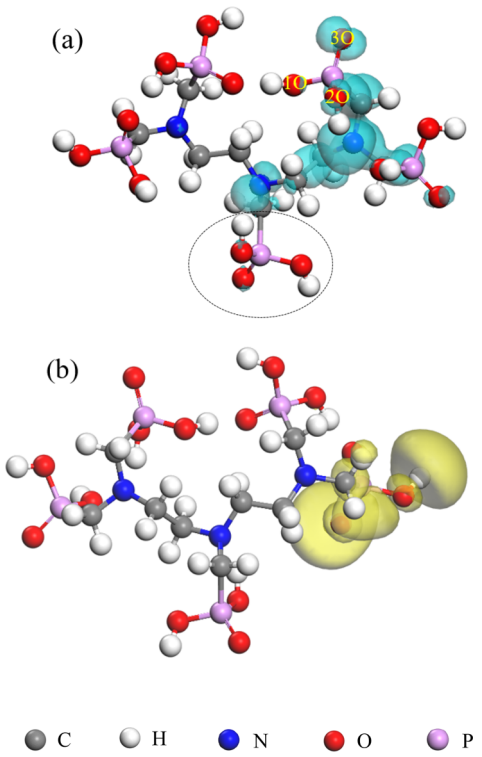

Figure 11. (a) HOMO and (b) LUMO of DTPMPA (DM).

greatly increase the probability of forming covalent bonds with DM. However, in this study, the calcium atoms interacting with the fluorite and calcite surfaces do not have abundant d-orbital electrons, indicating that the LUMO orbital of the inhibitor DM molecules has little effect on mineral interaction.

The DFT method was used to conduct the Mulliken charge analysis after optimizing the DM, as presented in Table 1. The

Table 1. Mulliken Charge after DTPMPA (DM) Optimization Calculation

atomic type	N	P	1O	2O	3O
electronic (e)	−0.296	1.572	−0.606	−0.701	−0.715

Mulliken charge of a pharmaceutical molecule indicates the charge distribution of its constituent atoms.[31] As observed from the table and in conjunction with the previous analysis of the HOMO orbital, the negative charge is primarily localized on the phosphate group on the HOMO orbital. As Figure 11a illustrates, the negative charge is concentrated on the O atom of the No. 2 phosphate group and the O atom of the No. 3 phosphate group. The N atom charge on the HOMO orbital of the drug molecule and the H connected with the 2O on the phosphate group is weakly negative, and its electron donor capacity is weak.[46] Conversely, the phosphorus atom carries a positive charge and does not contribute electrons. It can therefore be inferred that the negative charge mainly resides on the 2O and 3O atoms of the HOMO orbital phosphate group, signifying them to be the primary electron-donating centers in DM molecules. Since all phosphate groups in DM are equivalent, the charge distribution among atoms in the molecule will be transferred during the optimization process. Notably, the O atom in the phosphate group readily donates electrons, activating the calcite surface. Given the high density of Ca and the presence of empty orbitals on the calcite (104) surface, Ca readily accepts the donated electrons from the phosphate group O atom in DM. As shown in Table 1, the O atom in the inhibitor phosphate group exhibits a strong electron-donating ability to the metal present on the mineral surface.[31] Furthermore, the interaction between the atom of the phosphate group of DM and the Ca atom on the calcite (104) surface enables the inhibitor molecule to exert its effects specifically on the calcite (104) surface.

3.5.2. Equilibrium Configurations and Adsorption Energies. The adsorption of DM on the calcite (104) surface and the fluorite (111) surface was investigated using DFT. An ultrasoft pseudopotential was utilized for the calculations.[47] Figure 12 illustrates a 3 × 3 × 1 supercell model of the calcite (104) surface composed of six atomic layers. During the surface optimization process, the three layers of atoms at the bottom were kept fixed, unlike the other layers. A 25 Å vacuum layer was added. The layer was in the *z*-direction. A 400 eV cutoff energy was used for the plane wave basis expansion, with a 1.0×10^{-5} eV/atom energy convergence tolerance, 4.0×10^{-2} eV/Å force convergence tolerance, and 1.0×10^{-3} Å maximum displacement convergence tolerance. The Monkhorst−Pack scheme at a setting of 1 × 2 × 1 was used to conduct the K-point grid sampling. Additionally, the DFT-D correction method was used to account for remote van der Waals interactions.[48] The optimized surface structure of calcite (104), as depicted in Figure 12b, was obtained. The surface construction and optimization parameters for the fluorite (111) surface agreed with those of the calcite (104) surface. For the molecular optimization of DM, an ultrasoft pseudopotential was used. A 400 eV plane wave expansion cutoff energy was used. The convergence criteria were 1.0 ×

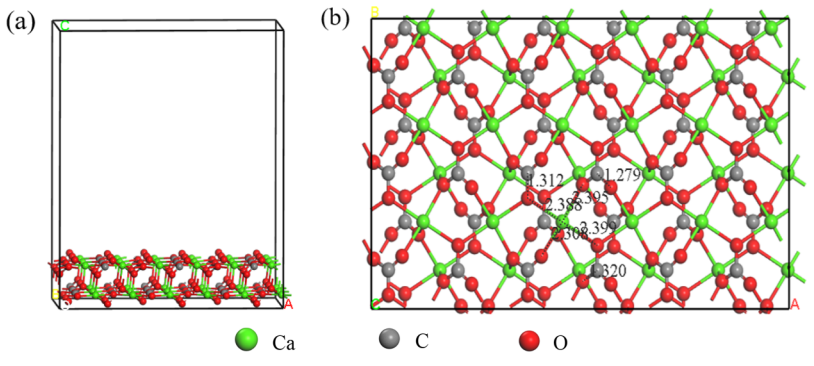

Figure 12. (a) Optimized calcite (104) crystal face main view and (b) calcite (104) crystal face top view.

https://doi.org/10.1021/acsomega.3c10400
ACS Omega 2024, 9, 17354−17367

10^{-5} eV/atom, 4.0×10^{-2} eV/Å, and 1.0×10^{-3} Å for energy, force, and maximum displacement, respectively, to obtain the optimal structure of the DM inhibitor (Figure 13). Figures 13 and 14 illustrate the optimization of the adsorption configuration of DTPMPA on the calcite (104) surface and fluorite (111) surface in the absence of water.

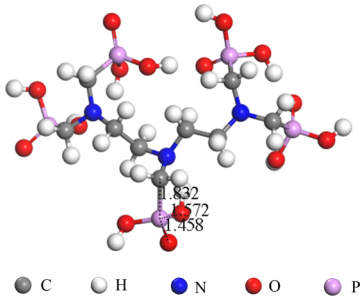

Figure 13. Molecular structure of EDTMPA (DM) after optimization.

DM on the calcite surface has three adsorption models: the coordination of a single oxygen and a single calcium atom (see Figure 14a), the coordination of double oxygen atoms and a single calcium atom (see Figure 14b), and the coordination of double oxygen atoms and double calcium atoms (see Figure 14c).[49−51] The adsorption model after optimization is displayed in Figure 14, and Table 2 presents the corresponding adsorption energies. As Table 2 shows, the interaction energy for all three models is negative, indicating their plausibility.

The organic molecules are bridged with the mineral surface (the active coordination atoms of the pharmaceutical molecules are bridged with the metal ions on the mineral surface and form a ring structure) and the geometric structure of the monodentate conformation. Figure 14 shows that DM exhibits three adsorption configurations on the calcite surface. These configurations include a monodentate mononuclear structure where one oxygen atom from the phosphate group of the chemical molecule is adsorbed onto a calcium atom on the calcite surface (Figure 14a); a bidentate mononuclear structure where two oxygen atoms from the phosphate group of the chemical molecule are adsorbed onto a calcium atom on the calcite surface (Figure 14b); and a bidentate binuclear complex structure where two oxygen atoms from the phosphate group of the pharmaceutical molecule are adsorbed onto two Ca atoms on the calcite surface (104) (Figure 14c).[52]

In these three adsorption models, both the P═O and P−O bonds in the drug molecules as well as the Ca−O bonds on the calcite surface are elongated. This indicates the activation of the phosphoric acid groups of the DM drug molecules during the adsorption process along with the activation of the calcite surface. Figure 14a shows that the length of the Ca−O bond formed by the adsorption of DM and Ca atoms on the calcite surface is 0.2241 nm, which is less than the sum of atomic radii (0.2630 nm), thus confirming chemical adsorption. Table 2 demonstrates the spontaneous reactivity of DM on the calcite surface. Figure 14b shows that the phosphate groups P═O and P−O are adsorbed onto the Ca surface of calcite, forming a stable bidentate mononuclear four-membered ring adsorption structure. The length of the Ca−O bond formed by the adsorption of P−O and Ca was 0.2490 nm, falling within the range of the calcite Ca−O bonds (0.2356, 0.2420, 0.2447, and 0.2663 nm), which indicates relative stability. However, the length of the Ca−O bond formed by O and Ca on P═O was 0.2736 nm, exceeding the sum of atomic radii for Ca−O (0.2630 nm), rendering it unstable. In Figure 14c, this is caused by the bidentate binuclear pentacyclic ring configuration formed by the combination of P═O of the phosphate group on the pharmaceutical molecule and P−OH with two Ca atoms on calcite. The length of the O−Ca bond formed by the P═O of the phosphate group on the pharmaceutical molecule and O on P−OH with two Ca atoms on calcite was 0.2347 and 0.2510 nm, respectively. All the Ca−O bonds on the calcite surface were in the range of 0.2316−0.2571 nm, and the Ca−O bonds formed were shorter than the sum of the atomic radii (0.2630 nm).

Furthermore, the adsorption energy of these three adsorption configurations of DM on the upper surface of calcite was calculated using Materials Studio for comparison. A higher adsorption energy negativity corresponds to a more stable adsorption structure.[53−55] As Table 1 shows, the adsorption energy ΔE_{ads} of the bidentate binuclear configuration was −192.39 kJ/mol. The adsorption energy ΔE_{ads} of the bidentate mononuclear configuration was −138.80 kJ/mol, and the adsorption energy ΔE_{ads} of the monodentate mononuclear configuration was −95.50 kJ/mol. By comparing the three configurations, we observe that ΔE_{ads} of the bidentate binuclear configuration $<\Delta E_{ads}$ of the bidentate mononuclear $<\Delta E_{ads}$ of the monodentate mononuclear configuration. Therefore, the bidentate binuclear configuration exhibits the most stable adsorption, followed by the mononuclear configuration. This conclusion is consistent with previous analyses.

Figure 15 shows the bidentate binuclear configuration of DM adsorbed on the fluorite surface. When chelating inhibitor molecules are adsorbed on the surface of calcite, the most stable adsorption configuration is the bidentate binuclear model. The bidentate binuclear adsorption configurations of the chelating inhibitor DM on the fluorite and calcite surfaces were compared. As Table 2 shows, the adsorption energy ΔE_{ads} of DM acting on the surface of fluorite in the bidentate binuclear configuration was −138.13 kJ/mol. This means that the agent was adsorbed on fluorite. In terms of the adsorption energy, the adsorption strength of DM on fluorite was not as strong as that on calcite. The lengths of the O−Ca bonds formed by the chelating inhibitor DM during adsorption on the surface of fluorite were 0.2403 and 0.2323 nm, respectively, indicating that the adsorption was relatively stable. This may be because the density of the Ca^{2+} site on the surface of fluorite (12.87 μmol/m^2) was higher than that on the surface of calcite (8.22 μmol/m^2). Furthermore, DM adsorption on the calcite mineral surfaces was affected. In general, DM also had an adsorption effect on the surface of fluorite, which was reflected in the experimental and simulation calculations. Upon the simultaneous addition of DM and NaOl, NaOl exhibited preferential adsorption on fluorite, occupying the active sites and hindering the adsorption of DM. The capacity of DM to be adsorbed on fluorite was lower than that of calcite; thus, DM was adsorbed first on the calcite surface.

The above data prove that the oxygen−calcium interaction peaks in the bidentate binuclear adsorption model. This model is a five-membered ring structure, which is also the most stable adsorption structure for DM and calcite. In conclusion, the simulated data confirmed that the adsorption of DM on calcite can be classified as a strong chemical adsorption, aligning with previous analyses conducted by using FTIR and XPS.

https://doi.org/10.1021/acsomega.3c10400
ACS Omega 2024, 9, 17354−17367

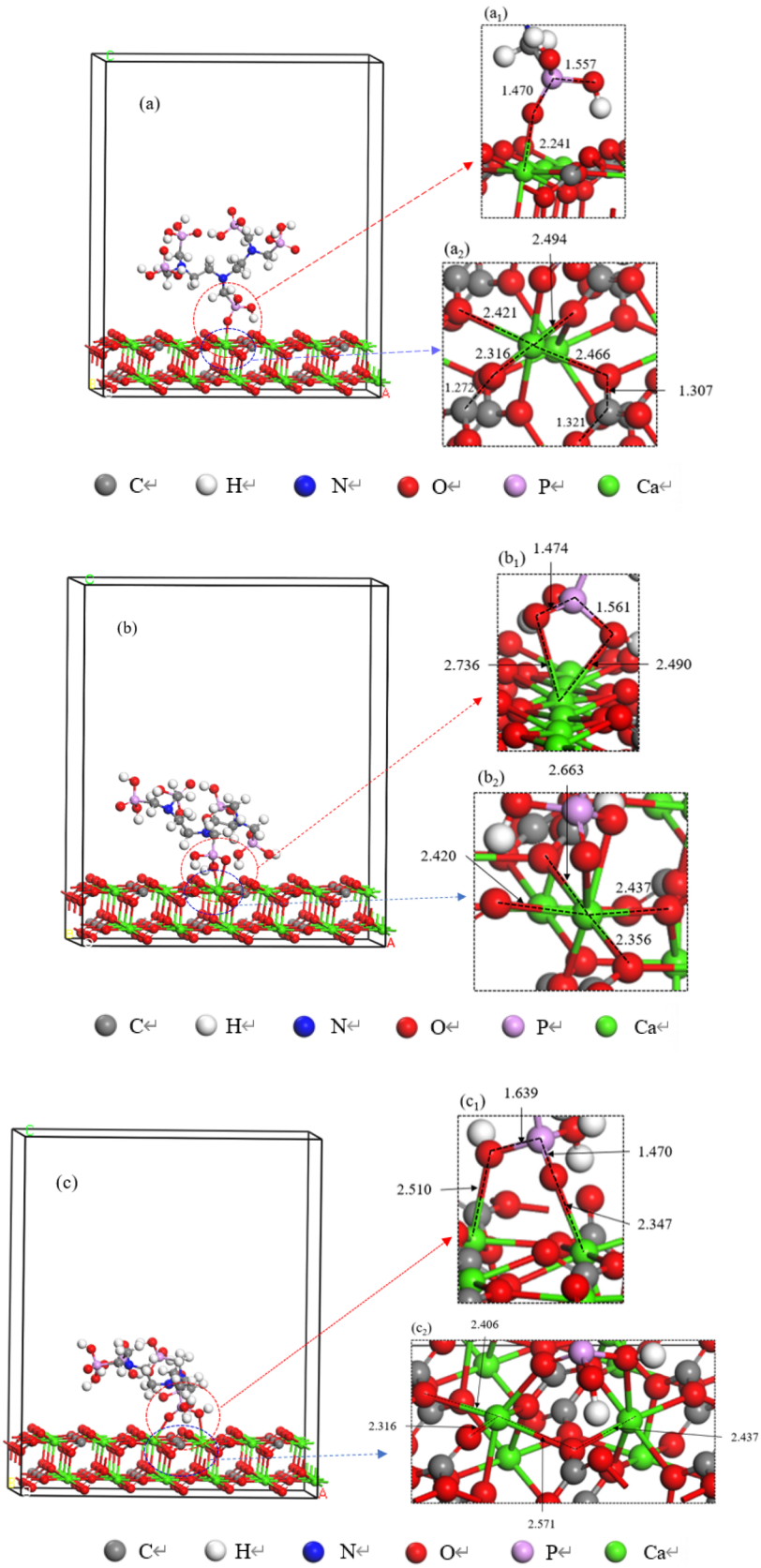

Figure 14. Three adsorption models: (a) optimally balanced by DTPMPA (DM) on the calcite (104) plane (monodentate mononuclear equilibrium configuration), (b) bidentate mononuclear equilibrium configuration, and (c) bidentate binuclear equilibrium configuration.

3.5.3. Density of States Analysis. To investigate the interaction between the inhibitor DM and the surfaces of calcite (104) minerals, the total density of states (TDOS) and partial density of states (PDOS) prior to and following the

https://doi.org/10.1021/acsomega.3c10400
ACS Omega 2024, 9, 17354−17367

Table 2. Adsorption Energy of DTPMPA (DM) in Different Adsorption Models on the Calcite Surface

minerals	adsorption models	adsorption energy/(kJ/mol)
calcite	monooxygen and monocalcium	−95.50
	double oxygen and single calcium	−138.80
	double oxygen and double calcium	−192.39
fluorite	double oxygen and double calcium	−138.13

inhibitor's adsorption onto the mineral surfaces were obtained using DFT.[56,57] The TDOS and PDOS of the inhibitor DM before and after its adsorption onto the calcite (104) surfaces were compared.

Figure 16a presents the total surface density and surface atomic density of $CaCO_3$. As the figure illustrates, certain DOS exhibit orbital contributions from Ca 4s, O 2p, and the C 2p. The valence band primarily consists of O 2p states with negligible input from Ca 4s. Previous research results have indicated that the surface of calcite is predominantly composed of Ca, and the valence state of Ca in the unoptimized structure is $3s^2 3p^6 4s^2$, with no contribution from the 3d orbitals. Nevertheless, the optimized structure introduces 3d orbitals into the conduction band, although their contribution is minimal. These 3d orbitals mainly aid in transferring charges from the 4s orbital state to the inhibitor's C and O orbitals. Therefore, the dominant orbitals are the 4s orbitals of Ca.[58] As Figure 16a illustrates, the optimized structure demonstrates noticeable contribution of the Ca 4s orbital in the conduction band within the energy range of 4.2−10 eV. This indicates that the Ca 4s orbital on the surface of calcite carries a predominantly positive charge, facilitating easy transfer of atoms, which aligns with findings in the literature and highlights the strong reactivity of Ca on the calcite surface.

Figure 16b illustrates the distribution of the TDOS for the adsorbed reagent and mineral is presented, while the partial density of states diagram is shown in Figure 16c. A Fermi level (E_f) of 0 eV was used, as depicted in the figures.[59] Figure 16b shows that when the inhibitor acts on the surface of $CaCO_3$, the peak of the TDOS reduces and the Fermi level increases. This suggests that because of the action of the inhibitor DM, calcite becomes more prone to electron acceptance, thereby enhancing the oxidation capacity of the calcite surface.[60] These findings indicate an increased activity of Ca on the calcite (104) surface. The emergence of new TDOS peaks within the ranges of −10 to −9 eV, −9.8 to 8.5 eV, −6 to −4.3 eV, and −1.9 to 0.2 eV (indicated by orange dashed boxes) further confirms the interaction of the inhibitor DM with the calcite surface.

In Figure 16c, the purple dotted line indicates that the O 2p and C 2p orbits overlap significantly at −9.8 to −8.5 eV and −6 to −4.3 eV, where the roles of C and O are unclear. The black dotted line denotes partial overlap between the O 2p and Ca 4s orbitals, specifically at −9 to −8.5 eV, with notable overlaps observed between higher energy levels of 3 to 5 eV. This indicates a strong interaction between the O atoms and Ca atoms, suggesting that the overlap between carbon and oxygen may be a product of the Ca−O interaction. This finding aligns with previous findings[57] and supports the conclusion that there is a strong bond between O and Ca. The above observation indicates a strong interaction between the phosphate group of the O atom and the calcite surface Ca atom, which agrees with the XPS analyses presented in Figure 10. The interaction between the O atom in DM phosphoric acid and the Ca atom on the calcite surface forms a stable chemical bond, which plays a leading role in the calcite surface adsorption, as is similarly shown in Figure 14c. Specifically, DM has a higher tendency to be adsorbed on the calcite surface to form stable chelating compounds than on the surface of two minerals.

4. CONCLUSIONS

In this study, diethylene triamine penta methyl phosphonic acid (DTPMPA) was used as a novel inhibitor for calcite, while sodium oleate was used as the flotation collector. At a dosage of 1.5×10^{-4} mol/L and a pH = 8, DTPMPA exhibited selective inhibition toward calcite, with a recovery rate of only 20.34% compared to a considerably higher recovery rate of 81.73% for fluorite. The interaction between DTPMPA and the calcite surface was further examined by using zeta potential measurements, Fourier transform infrared spectroscopy, and X-ray photoelectron spectroscopy. The findings revealed the strong chemisorption of DTPMPA on the calcite surface; however, DTPMPA exhibited physical adsorption on the fluorite surface. Furthermore, the frontier molecular orbital

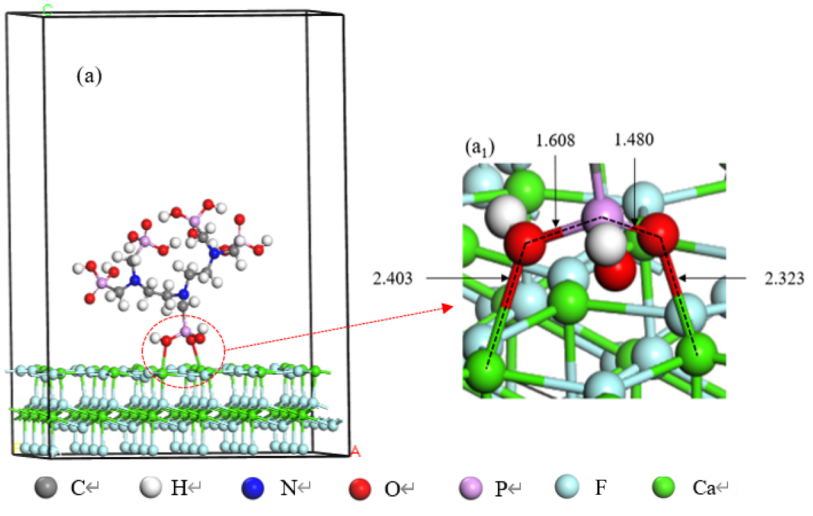

Figure 15. DTPMPA (DM) adsorption on the fluorite (111) surface of the bidentate binuclear equilibrium configuration.

https://doi.org/10.1021/acsomega.3c10400
ACS Omega 2024, 9, 17354−17367

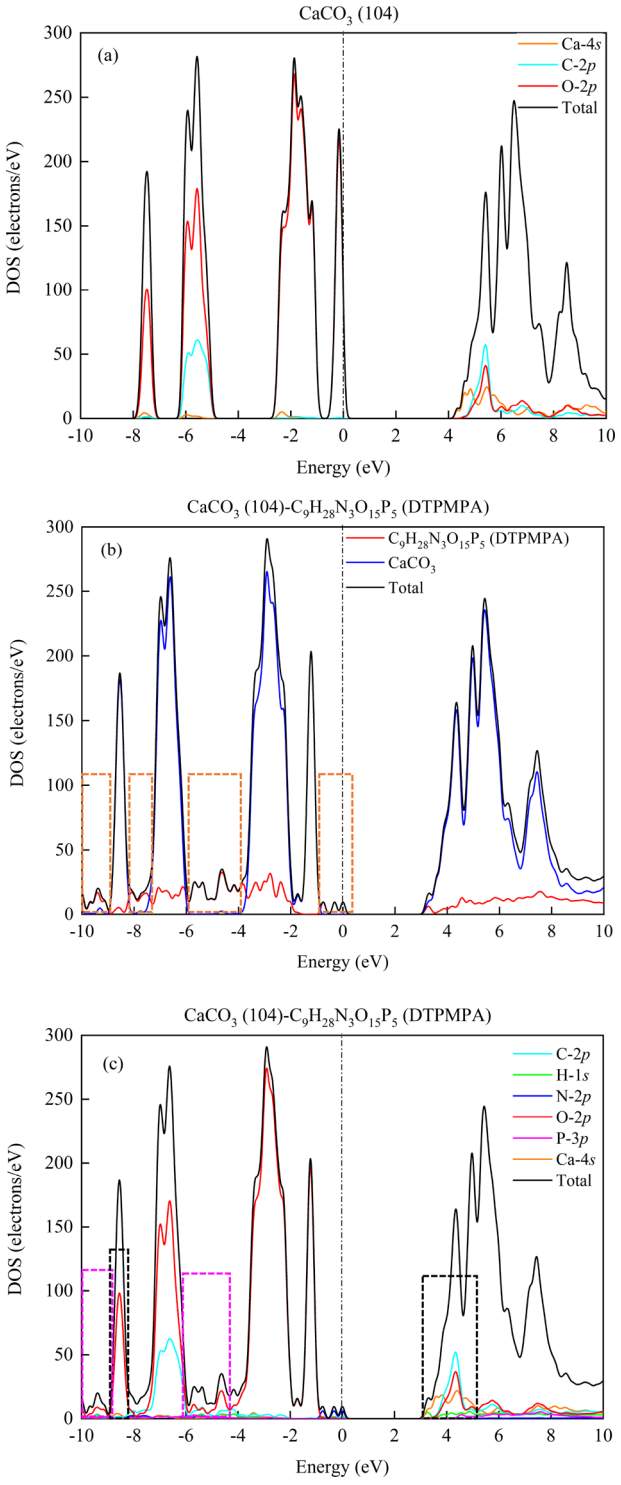

Figure 16. (a) Density of states diagram of $CaCO_3$ (104). (b) Total density of states diagram DTPMPA (DM) adsorbed on the surface of $CaCO_3$ (104). (c) Partial density of states diagram of DTPMPA (DM) adsorbed on the surface of calcite (104).

analysis and Mulliken population analysis showed that the O atom in the phosphoric acid group serves as the reactive center for DTPMPA. Comparing the three adsorption configurations showed that the lowest adsorption energy of the inhibitor on calcite is the bidentate binuclear structure and that chelation is most stable with a five-membered ring structure. The TDOS and PDOS results confirmed that the phosphate group of DTPMPA and Ca on the surface of calcite formed a stable chemical bond through charge transfer, which realized the effective separation of fluorite and calcite. This work provides significant guidance for the application of calcite flotation chelate inhibitors.

AUTHOR INFORMATION

Corresponding Author

Chenhu Zhang − *School of Mining and Mechanical Engineering, Liupanshui Normal University, Liupanshui, Guizhou 553004, China;* orcid.org/0009-0004-6349-2345; Email: lupin626@163.com

Authors

Haijun Wu − *College of Environmental and Chemical Engineering, Dalian University, Dalian, Liaoning 116622, China; School of Mining and Mechanical Engineering, Liupanshui Normal University, Liupanshui, Guizhou 553004, China*

Jing Zhang − *College of Environmental and Chemical Engineering, Dalian University, Dalian, Liaoning 116622, China*

Chengyong Wang − *School of Mining and Mechanical Engineering, Liupanshui Normal University, Liupanshui, Guizhou 553004, China;* orcid.org/0000-0003-0771-4068

Peng Chen − *School of Mining and Mechanical Engineering, Liupanshui Normal University, Liupanshui, Guizhou 553004, China*

Shiwei Wang − *School of Mining and Mechanical Engineering, Liupanshui Normal University, Liupanshui, Guizhou 553004, China*

Complete contact information is available at: https://pubs.acs.org/10.1021/acsomega.3c10400

Author Contributions

H.W.: experiment, formal analysis, writing—original draf; C.Z.: methodology, resources, project administration, writing—review; J.Z.: investigation, conceptualization; C.W.: conceptualization, writing—review and editing; P.C.: investigation, writing—review and editing; S.W.: investigation, conceptualization. All authors have read and agreed to the published version of the manuscript.

Notes

The authors declare no competing financial interest.

ACKNOWLEDGMENTS

The authors would like to acknowledge the financial support provided by the Innovation Team Foundation of Education Department of Guizhou Province (qian jiao ji [2023]087), the National Natural Science Foundation of Guizhou Province (Qiankehejichu-ZK [2022] Yiban 532), the National Natural Science Foundation of China (52264032), and the Fund of Liupanshui Normal University (LPSSY2023XKTD01, LPSSYLPY202223). The authors extend their gratitude to Theoretical and Computational Chemistry Team from Shiyanjia Lab (www.shiyanjia.com) for providing invaluable assistance in the simulation part.

REFERENCES

(1) Gao, Z.; Gao, Y.; Zhu, Y.; Hu, Y.; Sun, W. Selective flotation of calcite from fluorite: a novel reagent schedule. *Minerals* **2016**, *6* (4), 114.

https://doi.org/10.1021/acsomega.3c10400
ACS Omega 2024, 9, 17354−17367

(2) Corpas-Martínez, J. R.; Pérez, A.; Navarro-Domínguez, R.; Amor-Castillo, C.; Martín-Lara, M.; Calero, M. Comparison between performance of fluorite flotation under different depressants reagents in two pieces of laboratory equipment. *Applied Sciences* **2020**, *10* (16), 5667.
(3) Jiang, W.; Gao, Z.; Khoso, S. A.; Gao, J.; Sun, W.; Pu, W.; Hu, Y. Selective adsorption of benzhydroxamic acid on fluorite rendering selective separation of fluorite/calcite. *Appl. Surf. Sci.* **2018**, *435*, 752−758.
(4) Asadi, M.; Mohammadi, M. T.; Moosakazemi, F.; Esmaeili, M.; Zakeri, M. Development of an environmentally friendly flowsheet to produce acid grade fluorite concentrate. *Journal of Cleaner Production* **2018**, *186*, 782−798.
(5) Pugh, R.; Stenius, P. Solution chemistry studies and flotation behaviour of apatite, calcite and fluorite minerals with sodium oleate collector. *Int. J. Miner. Process.* **1985**, *15* (3), 193−218.
(6) Cao, Z.-F.; Zhong, H.; Song, Y.; Liu, G.-Y.; Wang, S.; Xia, L.-Y. Technological mineralogy of fluorite ore and its flotation performance. *Zhongguo Kuangye Daxue Xuebao* **2012**, *41* (3), 439−445.
(7) Zhu, W.; Pan, J.; Yu, X.; He, G.; Liu, C.; Yang, S.; Zeng, Y.; Zeng, A.; Liu, T. The flotation separation of fluorite from calcite using hydroxypropyl starch as a depressant. *Colloids Surf., A* **2021**, *616*, No. 126168.
(8) Gao, Z.; Wang, C.; Sun, W.; Gao, Y.; Kowalczuk, P. B. Froth flotation of fluorite: A review. *Advances in colloid and interface science* **2021**, *290*, No. 102382.
(9) Lopez Valdivieso, A.; Sánchez López, A.; Song, S.; García Martínez, H.; Licón Almada, S. Dextrin as a regulator for the selective flotation of chalcopyrite, galena and pyrite. *Canadian Metallurgical Quarterly* **2007**, *46* (3), 301−309.
(10) Dong, L.; Jiao, F.; Qin, W.; Liu, W. Selective flotation of scheelite from calcite using xanthan gum as depressant. *Minerals Engineering* **2019**, *138*, 14−23.
(11) Guo, W.; Feng, B.; Zhong, Z.; Weng, C.; Luo, X. Research progress on the depressants for flotation separation of scheelite and calcium-bearing gangue. *Conserv. Util. Min. Resour.* **2017**, *4*, 113−118.
(12) Song, S.; Lopez-Valdivieso, A.; Martinez-Martinez, C.; Torres-Armenta, R. Improving fluorite flotation from ores by dispersion processing. *Minerals Engineering* **2006**, *19* (9), 912−917.
(13) Zhang, C.; Wei, S.; Hu, Y.; Tang, H.; Gao, J.; Yin, Z.; Guan, Q. Selective adsorption of tannic acid on calcite and implications for separation of fluorite minerals. *J. Colloid Interface Sci.* **2018**, *512*, 55−63.
(14) Omae, I. Intramolecular five-membered ring compounds and their applications. *Coord. Chem. Rev.* **2004**, *248* (11−12), 995−1023.
(15) Omae, I. Applications of five-membered ring products of cyclometalation reactions as anticancer agents. *Coord. Chem. Rev.* **2014**, *280*, 84−95.
(16) Omae, I. Applications of cyclometalation reaction five-membered ring products. *J. Organomet. Chem.* **2018**, *869*, 88−105.
(17) Geffroy, C.; Foissy, A.; Persello, J.; Cabane, B. Surface complexation of calcite by carboxylates in water. *J. Colloid Interface Sci.* **1999**, *211* (1), 45−53.
(18) Zhang, C.; Wu, H.; Sun, W.; Hu, Y.; Wang, C.; Zhu, S.; Chen, P. Investigation of the flotation separation of scheelite from fluorite with a novel chelating agent: Pentasodium diethylenetriaminepentaacetate. *Minerals* **2022**, *12* (5), 530.
(19) Chen, Y.; Tang, X. Selective flotation separation of smithsonite from calcite by application of amino trimethylene phosphonic acid as depressant. *Appl. Surf. Sci.* **2020**, *512*, No. 145663.
(20) Zhu, Y.; Li, H.; Zhu, M.; Wang, H.; Li, Z. Dynamic and active antiscaling via scale inhibitor pre-stored superhydrophobic coating. *Chemical Engineering Journal* **2021**, *403*, No. 126467.
(21) Zeino, A.; Albakri, M.; Khaled, M.; Zarzour, M. Comparative study of the synergistic effect of ATMP and DTPMPA on CaSO4 scale inhibition and evaluation of induction time effect. *Journal of Water Process Engineering* **2018**, *21*, 1−8.
(22) Foucaud, Y.; Badawi, M.; Filippov, L. O.; Filippova, I. V.; Lebegue, S. Surface properties of fluorite in presence of water: An atomistic investigation. *J. Phys. Chem. B* **2018**, *122* (26), 6829−6836.
(23) Foucaud, Y.; Lebègue, S.; Filippov, L. O.; Filippova, I. V.; Badawi, M. Molecular insight into fatty acid adsorption on bare and hydrated (111) fluorite surface. *J. Phys. Chem. B* **2018**, *122* (51), 12403−12410.
(24) Lardge, J. S.; Duffy, D.; Gillan, M. Investigation of the interaction of water with the calcite (10.4) surface using ab initio simulation. *J. Phys. Chem. C* **2009**, *113* (17), 7207−7212.
(25) Speziale, S.; Duffy, T. S. Single-crystal elastic constants of fluorite (CaF 2) to 9.3 GPa. *Physics and Chemistry of Minerals* **2002**, *29*, 465−472.
(26) Gao, Y. -s.; Gao, Z. -y.; Sun, W. A review of anisotropic surface properties of fluorite. *Chin. J. Nonferrous Met* **2016**, *26*, 415−422.
(27) Chichagov, A. Information-calculating system on crystal structure data of minerals (MINCRYST). *Mater. Sci. Forum* 1994, 193−198. DOI: 10.4028/www.scientific.net/msf.166-169.193
(28) Gao, Z. -Y.; Wei, S.; Hu, Y. -H.; Liu, X. -W. Surface energies and appearances of commonly exposed surfaces of scheelite crystal. *Trans. Nonferrous Met. Soc. China* **2013**, *23* (7), 2147−2152.
(29) Wu, J.; Ma, W.; Wang, X.; Jiao, F.; Qin, W. The effect of galvanic interaction between chalcopyrite and pyrite on the surface chemistry and collector adsorption: Flotation and DFT study. *Colloids Surf., A* **2020**, *607*, No. 125377.
(30) Li, L.; Zhang, C.; Yuan, Z.; Xu, X.; Song, Z. AFM and DFT study of depression of hematite in oleate-starch-hematite flotation system. *Appl. Surf. Sci.* **2019**, *480*, 749−758.
(31) Gao, Z.; Deng, J.; Sun, W.; Wang, J.; Liu, Y.; Xu, F.; Wang, Q. Selective flotation of scheelite from calcite using a novel reagent scheme. *Mineral Processing and Extractive Metallurgy Review* **2022**, *43* (2), 137−149.
(32) Xu, Y.; Xu, L.; Wu, H.; Tian, J.; Wang, Z.; Gu, X. The effect of citric acid in the flotation separation of bastnaesite from fluorite and calcite using mixed collectors. *Appl. Surf. Sci.* **2020**, *529*, No. 147166.
(33) Filippova, I.; Filippov, L.; Duverger, A.; Severov, V. Synergetic effect of a mixture of anionic and nonionic reagents: Ca mineral contrast separation by flotation at neutral pH. *Minerals Engineering* **2014**, *66*, 135−144.
(34) Zhu, H.; Qin, W.; Chen, C.; Chai, L.; Jiao, F.; Jia, W. Flotation separation of fluorite from calcite using polyaspartate as depressant. *Minerals Engineering* **2018**, *120*, 80−86.
(35) Chen, W.; Feng, Q.; Zhang, G.; Yang, Q. Investigations on flotation separation of scheelite from calcite by using a novel depressant: Sodium phytate. *Minerals Engineering* **2018**, *126*, 116−122.
(36) Haney, R.; Siddiqui, N.; Andress, J.; Fergus, J.; Overfelt, R.; Prorok, B.Principal component analysis (PCA) application to FTIR spectroscopy data of CO/CO2 contaminants of air. In *41st International Conference on Environmental Systems*; AIAA 2011; p 5091.
(37) Gao, Z.; Li, C.; Sun, W.; Hu, Y. Anisotropic surface properties of calcite: A consideration of surface broken bonds. *Colloids Surf., A* **2017**, *520*, 53−61.
(38) Zhu, X.; Huang, Y.; Zhu, Y.; Sun, N.; Wang, W. Investigating the performance of oxalic acid for separating bastnaesite from calcium-bearing gangue minerals based on experiment and theoretical calculation. *Minerals Engineering* **2021**, *170*, No. 107047.
(39) Azizi, D.; Larachi, F. Immiscible dual ionic liquid-ionic liquid mineral separation of rare-earth minerals. *Sep. Purif. Technol.* **2018**, *191*, 340−353.
(40) Liu, W.; Liu, W.; Zhao, Q.; Peng, X.; Wang, B.; Zhou, S.; Zhao, L. Investigating the performance of a novel polyamine derivative for separation of quartz and hematite based on theoretical prediction and experiment. *Sep. Purif. Technol.* **2020**, *237*, No. 116370.
(41) Wanhala, A. K.; Doughty, B.; Bryantsev, V. S.; Wu, L.; Mahurin, S. M.; Jansone-Popova, S.; Cheshire, M. C.; Navrotsky, A.; Stack, A. G. Adsorption mechanism of alkyl hydroxamic acid onto bastnäsite:

Fundamental steps toward rational collector design for rare earth elements. *J. Colloid Interface Sci.* **2019**, *553*, 210−219.
(42) Wei, Z.; Hu, Y.; Han, H.; Sun, W. Configurations of lead (II)−benzohydroxamic acid complexes in colloid and interface: A new perspective. *J. Colloid Interface Sci.* **2020**, *562*, 342−351.
(43) Fukui, K.; Yonezawa, T.; Shingu, H. A molecular orbital theory of reactivity in aromatic hydrocarbons. *J. Chem. Phys.* **1952**, *20* (4), 722−725.
(44) Sun, W.; Yang, F.; Hu, Y.; Liu, W. Applica- tion of frontier orbital in developing new collectors of chalcopyrite. *Chin. J. Nonferrous Metals* **2009**, *19* (8), 1524.
(45) Liu, G.; Xiao, J.; Zhou, D.; Zhong, H.; Choi, P.; Xu, Z. A DFT study on the structure-reactivity relationship of thiophosphorus acids as flotation collectors with sulfide minerals: Implication of surface adsorption. *Colloids Surf., A* **2013**, *434*, 243−252.
(46) Zhao, G.; Zhong, H.; Qiu, X.; Wang, S.; Gao, Y.; Dai, Z.; Huang, J.; Liu, G. The DFT study of cyclohexyl hydroxamic acid as a collector in scheelite flotation. *Minerals engineering* **2013**, *49*, 54−60.
(47) Kresse, G.; Joubert, D. From ultrasoft pseudopotentials to the projector augmented-wave method. *Physical review b* **1999**, *59* (3), 1758.
(48) Grimme, S.; Antony, J.; Ehrlich, S.; Krieg, H. A consistent and accurate ab initio parametrization of density functional dispersion correction (DFT-D) for the 94 elements H-Pu. *J. Chem. Phys.***2010**, *132* (15).
(49) Stumm, W. Reactivity at the mineral-water interface: dissolution and inhibition. *Colloids Surf., A* **1997**, *120* (1−3), 143−166.
(50) De Leeuw, N.; Parker, S.; Rao, K. H. Modeling the competitive adsorption of water and methanoic acid on calcite and fluorite surfaces. *Langmuir* **1998**, *14* (20), 5900−5906.
(51) Liu, J.; Xie, R.; Zhu, Y.; Li, Y.; Liu, C. Flotation behavior and mechanism of styrene phosphonic acid as collector on the flotation separation of fluorite from calcite. *J. Mol. Liq.* **2021**, *326*, No. 115261.
(52) Azizi, D.; Larachi, F. Surface interactions and flotation behavior of calcite, dolomite and ankerite with alkyl hydroxamic acid bearing collector and sodium silicate. *Colloids Surf., A* **2018**, *537*, 126−138.
(53) Valcárcel, A.; Clotet, A.; Ricart, J. M.; Delbecq, F.; Sautet, P. Comparative DFT study of the adsorption of 1, 3-butadiene, 1-butene and 2-cis/trans-butenes on the Pt (1 1 1) and Pd (1 1 1) surfaces. *Surface science* **2004**, *549* (2), 121−133.
(54) Xu, L.; Hu, Y.; Wu, H.; Tian, J.; Liu, J.; Gao, Z.; Wang, L. Surface crystal chemistry of spodumene with different size fractions and implications for flotation. *Sep. Purif. Technol.* **2016**, *169*, 33−42.
(55) Gong, G.; Wang, P.; Liu, J.; Han, Y.; Zhu, Y. Effect and mechanism of Cu (II) on flotation separation of cassiterite from fluorite. *Sep. Purif. Technol.* **2020**, *238*, No. 116401.
(56) Lemieux, M.-A.; Tremblay, A.-M. Densities of states, projected densities of states, and transfer-matrix methods from a unified point of view. *Phys. Rev. B* **1987**, *36* (3), 1463.
(57) Chai, R.; Liu, Y.; Liu, Q.; Xin, J. Interaction mechanism of calcite and four representative organic molecules: Experiments and DFT study. *Colloids Surf., A* **2021**, *612*, No. 125822.
(58) Hossain, F. M.; Murch, G. E.; Belova, I. V.; Turner, B. D. Electronic, optical and bonding properties of CaCO3 calcite. *Solid state communications* **2009**, *149* (29−30), 1201−1203.
(59) Han, Y.; Liu, W.; Chen, J. DFT simulation of the adsorption of sodium silicate species on kaolinite surfaces. *Appl. Surf. Sci.* **2016**, *370*, 403−409.
(60) Jiang, W.; Gao, Z.; Sun, W.; Gao, J.; Hu, Y. A density functional theory study on the effect of lattice impurities on the electronic structures and reactivity of fluorite. *Minerals* **2017**, *7* (9), 160.

https://doi.org/10.1021/acsomega.3c10400
ACS Omega 2024, 9, 17354−17367